Mechanical and self-healing properties of engineering cementitious capillary crystalline waterproofing materials-modified concrete

Jiao, Liying; Zhao, Sixue; Shang, Baiyu; Zhang, Zheng; Wan, Weifu; Zheng, Yongchao; Liu, Chen

DOI
10.1016/j.cscm.2025.e05552

Licence
CC BY

Publication date
2025

Document Version
Final published version

Published in
Case Studies in Construction Materials

Citation (APA)
Jiao, L., Zhao, S., Shang, B., Zhang, Z., Wan, W., Zheng, Y., & Liu, C. (2025). Mechanical and self-healing properties of engineering cementitious capillary crystalline waterproofing materials-modified concrete. *Case Studies in Construction Materials*, *23*, Article e05552. https://doi.org/10.1016/j.cscm.2025.e05552

Case Studies in Construction Materials 23 (2025) e05552

Contents lists available at ScienceDirect

Case Studies in Construction Materials

journal homepage: www.elsevier.com/locate/cscm

Case study

Mechanical and self-healing properties of engineering cementitious capillary crystalline waterproofing materials-modified concrete

Liying Jiao [a,b,1], Sixue Zhao [a,1], Baiyu Shang [b], Zheng Zhang [c], Weifu Wan [b], Yongchao Zheng [a], Chen Liu [d,*]

[a] Beijing Building Materials Acacemy of Sciences Research, Beijing 100041, China
[b] Beijing Jinyu Concrete Co., Ltd., Beijing 100165, China
[c] Beijing Tongzhou Investment Development Co., Ltd., Beijing 101125, China
[d] Department of Materials and Environment (Microlab), Faculty of Civil Engineering and Geoscience, Delft University of Technology, Delft, CN 2628, the Netherlands

ARTICLE INFO

Keywords:
CCCW
Self-healing
Active monitoring approach
Frequency shift
Healing effect

ABSTRACT

Cementitious capillary crystalline waterproofing materials (CCCW) can be used as a self-healing additive. Compared with other self-healing materials and methods, CCCW directly added to the concrete matrix is easier to apply in specific projects. In this study, long-life self-healing concrete was prepared for the Palace Museum North Campus project by adding expansion agents, polypropylene fibers, and CCCW. Its mechanical properties and durability were tested. At the same time, non-destructive testing methods were used to test the crack resistance and self-healing performance. The compressive strength was around 41 MPa (28 d) for C40 group and 47 MPa (28 d) for C45 group. The compressive strengths exhibited no loss after 300 freeze-thaw cycles. The results showed that CCCW reduces early cracking and exhibits a good repairing effect on cracks below 0.2 mm. The method provided a new technical route for evaluating the healing effect.

1. Introduction

As a widely utilized construction material, concrete is frequently exposed to complex and harsh operational environments. During service, microcracks are prone to form within the concrete matrix. If these microcracks propagate and induce matrix cracking, water and aggressive ions can infiltrate the interior more readily, accelerating corrosion of steel reinforcements and potentially triggering structural leakage [1,2]. In the case of the ongoing construction of the Northern Campus Project of the Palace Museum, any leakage would destabilize the internal temperature and humidity levels. Such instability, particularly recurrent fluctuations, significantly heightens the risk of corrosion or biodeterioration in cultural artifacts. This would critically degrade their preservation conditions and lifespan, thereby inflicting immeasurable harm on the heritage value of the Palace Museum's collections [3].

To ensure structural safety and meet low-carbon building requirements, it is imperative to reduce the possibility of concrete

* Corresponding author.
E-mail address: c.liu-12@tudelft.nl (C. Liu).
[1] Both Liying Jiao and Sixue Zhao are contributed equally to the work.

https://doi.org/10.1016/j.cscm.2025.e05552
Received 15 September 2025; Received in revised form 8 November 2025; Accepted 10 November 2025
Available online 21 November 2025

degradation and structural leakage caused by crack propagation [4-6]. However, the formation of cracks in concrete structures becomes inevitable with prolonged service time. Post-construction, addressing these cracks through manual repair necessitates the suspension of normal building operations and entails substantial economic costs. Consequently, the autonomous repair and monitoring of internal concrete cracks remain a critical challenge in civil engineering research [7,8].

Cementitious Capillary Crystalline Waterproofing Materials (CCCW) represent a category of rigid waterproofing materials [8,9] composed primarily of cementitious matrices supplemented with active chemical compounds [10,11]. When incorporated into the concrete matrix through internal mixing, the active constituents of CCCW partially dissolve in the pore solution. These water-soluble chemicals migrate through capillary pores, reacting with free calcium ions in the concrete pore solution to form stable precipitates. These precipitates effectively fill microporous structures, enhancing overall matrix densification and significantly improving impermeability [12–15]. Furthermore, in cracked concrete structures containing CCCW, unreacted active substances could participate in the reaction, generating additional precipitates that autonomously repair the cracks [16,17]. This dual functionality positions CCCW not only as a waterproofing agent but also as a self-healing additive capable of augmenting concrete's intrinsic autogenous repair capacity [18,19]. Notably, CCCW's material composition and fabrication processes are relatively uncomplicated. Compared to alternative self-healing materials, CCCW's direct integration into the concrete matrix via internal mixing offers superior practicality for large-scale engineering applications [20,21].

The ongoing Northern Campus Project of the Palace Museum employs CCCW incorporation and optimized mix proportion adjustments to achieve the design of long-lasting self-healing concrete. As an internally incorporated material, CCCW exerts significant impacts on concrete workability, necessitating adjustments to its compatibility with chemical admixtures [22]. Therefore, the proportion of high-quality fly ash was increased to 35 % to enhance workability, while slump-retaining components in the admixtures were augmented to improve compatibility. Additionally, the target concrete strength was strategically reduced, maintaining the strength redundancy coefficient below 1.2, thereby mitigating shrinkage in the concrete matrix.

Current methodologies such as the prefabricated crack method and water permeability tests are usually employed to evaluate CCCW's crack-repair efficacy [8]. However, these experimental approaches exhibit limited applicability in engineering and long-term performance monitoring. The study introduces a complementary non-destructive evaluation (NDE) technique for assessing concrete cracking and self-healing effectiveness. This methodology aims to provide sustainable technical support for the Northern Campus Project of the Palace Museum, ensuring lifecycle performance validation.

2. Materials and experimental design

2.1. Raw materials

The binder system utilized Portland cement (P.O. 42.5) produced by Chengde Jinyu Cement Co., Ltd., featuring an alkali content of 0.53 % and a specific surface area of 335 m^2/kg. Its chemical composition is detailed in Table 1. Aggregates included 0.5–2.3 mm machine-manufactured sand and 5–25 mm crushed stone. The main indicators of machine-manufactured sand and crushed stone are shown in Tables 1 and 2, respectively. Fly ash (chemical composition in Table 3) was incorporated as a supplementary cementitious material. The admixture system comprised a polycarboxylate-based water reducer and a Type II expansive agent, achieving a restricted expansion rate of 0.053 % in water at 7 days. Polypropylene fibers and CCCW (Kryton International Inc., Canada; technical parameters (tested according to GB18445–2021) in Table 4) were added, with the proprietary composition of CCCW undisclosed due to commercial confidentiality.

2.2. Mix design

The concrete in this project was designed with strength grades of C40 and C45. The C40 concrete was primarily employed for underground waterproofing structures, while the C45 grade was designed for structural post-pouring zones.

The design methodology implements a tri-phase (early-stage, mid-term, and long-term) full-lifecycle strategy to reduce crack mitigation, shrinkage reduction, and achieve autonomous repair in concrete. The mix proportion was designed with low cement content, high fly ash incorporation (35 % by mass of binder), and elevated coarse aggregate ratios [23]. This strategy achieves dual objectives of reducing carbon emissions and mitigating shrinkage [24]. To further enhance early-age crack resistance, polypropylene fibers (0.9 kg/m^3) were incorporated to minimize plastic shrinkage during the initial curing phase [25]. An expansive agent (Type II, 8 % by cement mass) was added to counteract cementitious shrinkage during early to mid-term hydration stages (1–14 days) [26]. CCCW was used to enable autonomous crack repair: when microcracks develop within the concrete matrix, reactive components in CCCW undergo secondary reactions with calcium-rich hydration products, generating insoluble crystallization products that seal internal voids and restore structural integrity.

Due to the impairment of concrete workability caused by the incorporation of multiple crack-resistant materials (polypropylene

Table 1
The main indicators of machine-manufactured sand.

Apparent density (kg/m^3)	Bulk density (kg/m^3)	Content of flake particles (wt%)	Fineness modulus	Stone powder content (wt%)
2620	1750	7.4 %	2.6	3.8 %

Table 2
The main indicators of crushed stone.

Apparent density (kg/m^3)	Bulk density (kg/m^3)	Void content (%)	Water Absorption (wt%)
2850	1530	46.2	2.8

Table 3
Chemical analysis of cement and fly ash.

Component/wt%	CaO	SiO_2	Al_2O_3	Fe_2O_3	MgO	SO_3	Cl^-	Loss	Total
Cement	58.10	20.80	7.14	3.31	3.84	2.35	0.05	2.36	99.87
Fly ash	5.38	49.32	35.88	3.87	1.11	0.33	0.01	0.04	99.90

Table 4
Technical parameters of CCCW.

Contents		Results
Chloride content /%		0.012
Compressive strength ratio/%	7d	112
	28d	106
Shrinkage ratio/%	28d	97
Impermeability pressure ratio/%	28d	200
	56d	167

fibers, expansive agents, and CCCW), the superplasticizer was compounded with fluidizing agents and slump-retaining components. This formulation achieved a slump of approximately 200 mm, meeting the pumpability requirements.

The C40 concrete mix exhibited a water-to-binder ratio of 0.39, while the C45 mix utilized a reduced ratio of 0.35 to achieve higher strength. The expansive agent was incorporated at 8 % by mass of the binder. Polypropylene fibers were added at a dosage of 0.9 kg/m^3 . During the experimental process, CCCW dosages of 1 % and 2 % by mass of the binder were selected for comparative evaluation. Detailed mix proportions for both concrete grades are summarized in Table 5 below.

2.3. Methods

For each mix proportion, specimens were cast and subjected to compressive strength testing at 7, 28 and 60 d curing ages. The 28 d specimens were utilized to evaluate frost resistance and drying shrinkage properties. The drying shrinkage behavior of concrete was measured via the contact method. After demolding at 1 d, the hardened concrete specimens were stored under controlled environmental conditions (temperature: 20 ± 2°C, relative humidity: 60 ± 5 %) to monitor shrinkage deformation at 1, 3, 7, 14, 28, 45, and 60 d.

Frost resistance testing employed the rapid freeze-thaw method (ASTM C666), where self-healing concrete specimens underwent 300 freeze-thaw cycles in water-ice-water transitions. The acceptance criteria required the relative dynamic elastic modulus to remain≥ 60 % and mass loss < 5 % after cycling.

Chloride ion permeability resistance was assessed via electrical flux testing (ASTM C1202–22) on 28 d cured specimens. Lower electrical flux values indicate higher compactness of the concrete matrix and a reduced risk of steel corrosion.

Mortar specimens with a 2 % CCCW dosage (by mass of binder) were cured under 99 % humidity and 20 ℃ for 3 days and 28 days for XRD and SEM analyses. Additionally, CCCW were mixed with water uniformly and cured under standard conditions for 28 days. XRD testing was conducted using a Rigaku Ultima IV X-ray diffractometer (Japan) with a scanning step size of 0.02°. For SEM observations, a Hitachi S-3400N scanning electron microscope (Japan) was employed to examine microstructural morphology.

Table 5
Mix proportions of concrete.

	w/c	CCCW /wt%	Material quantities per m^3 /kg								
			Water	Cem-ent	Sand	Stone	FA	Water reducer	Expa-nsive agent	Air-entraining agent	Fiber
C40–0	0.39	0	169	280	697	1090	125	9.5	30	0.5	0.9
C40–1	0.39	1.0	169	280	697	1090	125	9.5	30	0.5	0.9
C40–2	0.39	2.0	170	280	696	1089	125	10	30	0.6	0.9
C45–0	0.35	0	165	295	649	1105	140	11	35	0.5	0.9
C45–1	0.35	1.0	165	295	649	1105	140	11	35	0.5	0.9
C45–2	0.35	2.0	165	295	649	1105	140	11.5	35	0.6	0.9

2.4. The monitoring methods of self-healing effect

This article provides a method for non-destructive testing of concrete healing performance, with a view to providing long-term monitoring services for the Northern Campus Project of the Palace Museum. It is preferred to monitor the repair performance of C45 concrete with a CCCW content of 2 %, while selecting C45 concrete without CCCW as a control group for testing.

The tests were conducted with reference to the early crack resistance test method in ASTM C666. The concrete used was taken from the mixer truck and poured into a mold with a size of 800*600*100 mm. The bottom of the mold was equipped with a crack inducer. Immediately after molding, a fan was used to accelerate the formation of cracks. By adjusting the position and speed of the fan, the wind speeded at a height of 100 mm directly above the center of the test piece surface is set to (5 ± 0.5) m/s, as shown in Fig. 1.

The monitoring method employed piezoelectric sensors utilizing a wave propagation technique. The commercially available piezoelectric ceramic sensor array comprised an actuator (transmitter) and a receiver element. The experimental setup incorporated a signal generator (Rigol DG1022Z), a power amplifier (Sound Intelligence QXS-HPSA), and a dynamic signal acquisition system (Donghua DH5902G) to generate, amplify, and record ultrasonic waveforms, respectively.

The excitation signal was configured as a Hanning-windowed sinusoidal function with a central frequency of 50 kHz. Detailed signal parameters are listed in Table 6. Substituting these parameters into Eq. (1) modulates the sinusoidal signal into a Hanning-windowed form, as illustrated in Fig. 2(a). In Eq. (1), Y denotes signal amplitude, f represents the frequency (50 kHz), n indicates the number of cycles, and t corresponds to the sampling interval. Fourier transform analysis of the modulated Hanning signal (Fig. 2 (b)) reveals a monomodal spectral distribution, confirming effective time-domain to frequency-domain conversion with minimal spectral leakage.

$$Y = \frac{1}{2}(1 - \cos\left(\frac{2\pi ft}{n}\right)) \bullet \sin(2\pi ft) \tag{1}$$

The specimens were allowed to stabilize for 24 h after casting. Crack widths were measured using a micro-crack width gauge. The piezoelectric sensors were fixed by the epoxy resin adhesive, ensuring in-situ sensor immobilization throughout the monitoring period. The sensors were applied across cracks of varying widths at 10 cm intervals. As illustrated in Fig. 3, (a) represents the CCCW-modified group, while (b) denotes the control group. To simulate field moisture conditions, daily water spraying was performed on the surfaces to maintain consistent humidity levels for CCCW activation and hydration continuity.

3. Results

3.1. Concrete performance

The concrete performance is presented in Table 7. As shown in the table, all four mix proportions exhibited workable slump values (initial and 3-hour retained slump), meeting practical construction requirements. The 3 d compressive strength reached approximately 60 % of the design strength, while the 28d strength achieved 100 % of the design strength. At 60 d, the strength further developed to 119–121 % of the design strength, indicating a low strength overdesign coefficient. Notably, CCCW incorporation exhibited negligible impact on concrete strength. As evidenced by the compressive strength data, both C40 and C45 concrete mixes with varying CCCW dosages (1–2 % by binder mass) demonstrated statistically insignificant differences across all testing ages (7, 28, and 60 days).

Concurrently, both C40 and C45 concrete exhibited excellent impermeability, attributable to their highly dense matrix, which resulted in low electrical flux values. The incorporation of CCCW further reduced chloride ion permeability, with the electrical flux of C40 concrete decreasing by approximately 14.4 % at a 2 % CCCW dosage. Based on the 300 freeze-thaw cycles test, it was found that the addition of CCCW to C40 and C45 concrete can effectively improve its freeze-thaw resistance. The mass loss rate was below 5 %, and the relative dynamic modulus of elasticity decreased to a value of $\geq$ 70 %. This outcome validated the effectiveness of the multi-phase crack mitigation strategy (fibers, expansive agents, and CCCW) in preserving structural integrity under extreme environmental

Fig. 1. Testing process.

Table 6
Signal characteristics.

frequency (Hz)	sampling frequency (Hz)	signal cycle (s)	sampling interval (s)	Hanning cycles
50000	1000000	0.000025	0.000025	5

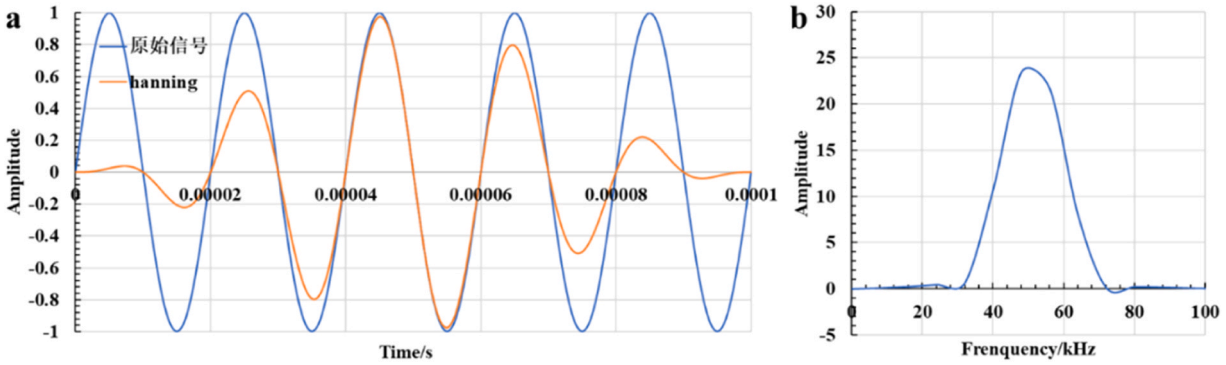

Fig. 2. Original signal and deformed signal.

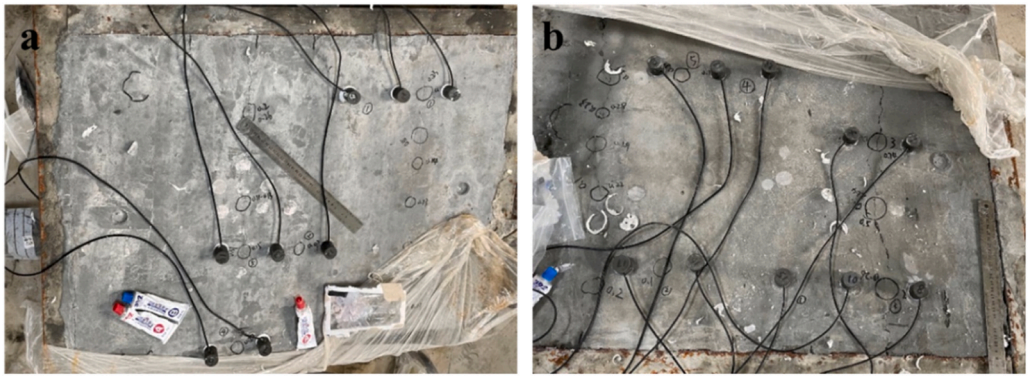

Fig. 3. Sensor pasting: (a) CCCW group, (b) blank group.

Table 7
The properties of concrete.

	Slump/expansion/mm		Compressive strength/MPa			Mass loss after 300 freeze-thaw cycles (%)	Relative dynamic modulus after 300 cycles (%)	60d electric flux/C
	initial	3 h	7d	28d	60d			
C40–0	230/540	220/520	26.8	41.2	50.2	5.3	67.2	725
C40–1	220/510	210/450	27.8	40.5	48.5	4.4	77.9	675
C40–2	225/540	190/400	27.6	41.5	49.3	4.7	74.6	578
C45–0	245/550	230/470	32.0	48.2	55.2	5.4	61.6	605
C45–1	230/520	210/440	30.2	46.7	54.3	3.7	72.3	565
C45–2	240/550	210/400	31.5	47.5	53.6	3.3	70.0	545

exposure.

The drying shrinkage of concrete at various ages (1, 3, 7, 14, 28, 45, and 60 d) is illustrated in Fig. 4. The results reveal a progressive increase in drying shrinkage values with aging. The C45 group exhibited the highest shrinkage of 234 με. Notably, at 1 d of age, the

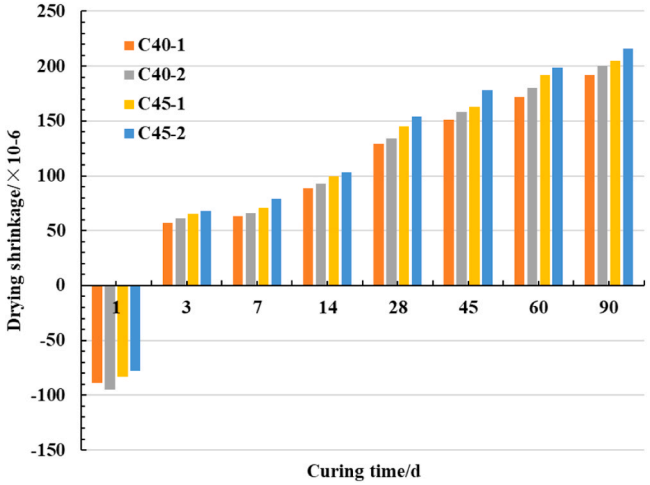

Fig. 4. Concrete drying shrinkage.

concrete displayed slight expansion, transitioning to shrinkage from 3 d onward. This phase shift underscores the critical role of water curing in enabling expansive agent activation during early hydration.

Furthermore, higher CCCW dosages exacerbated long-term shrinkage (60-day increase: 12–15 με per 1 % CCCW). This phenomenon arises from CCCW's internal water absorption during crystallization, which marginally amplifies desiccation-induced shrinkage under low-humidity conditions. To mitigate this effect, periodic surface moisture replenishment (daily spraying at 1.5 L/m^2) is recommended during the autonomous repair phase. For structural implementation, a minimum 14-day wet curing regime (RH ≥95 %, 20 ± 2°C) should be enforced to ensure full expansion potential and counteract early-age shrinkage.

3.2. The evaluation of self-healing effect

In this experiment, CCCW group exhibited significantly fewer macrocracks, with measurable crack widths lower than those of the control group. As shown in Figs. 5 and 6, the CCCW group consistently produced crack widths below 0.3 mm (Fig. 6), whereas the control group developed cracks ranging from 0 to 0.7 mm (Fig. 5), with a notable increase in cracks exceeding 0.5 mm in width. Initial signal monitoring demonstrated a clear correlation between crack width and piezoelectric response characteristics.

Fig. 7 presents the frequency-domain spectra of initial signals after Fourier transform analysis under varying crack widths. Key observations include: 1. Sub-0.1 mm cracks: For both CCCW and control groups, the dominant spectral peak remained within the original excitation frequency band (50 kHz), indicating minimal wave scattering; 2. 0.1–0.3 mm cracks: A progressive frequency shift

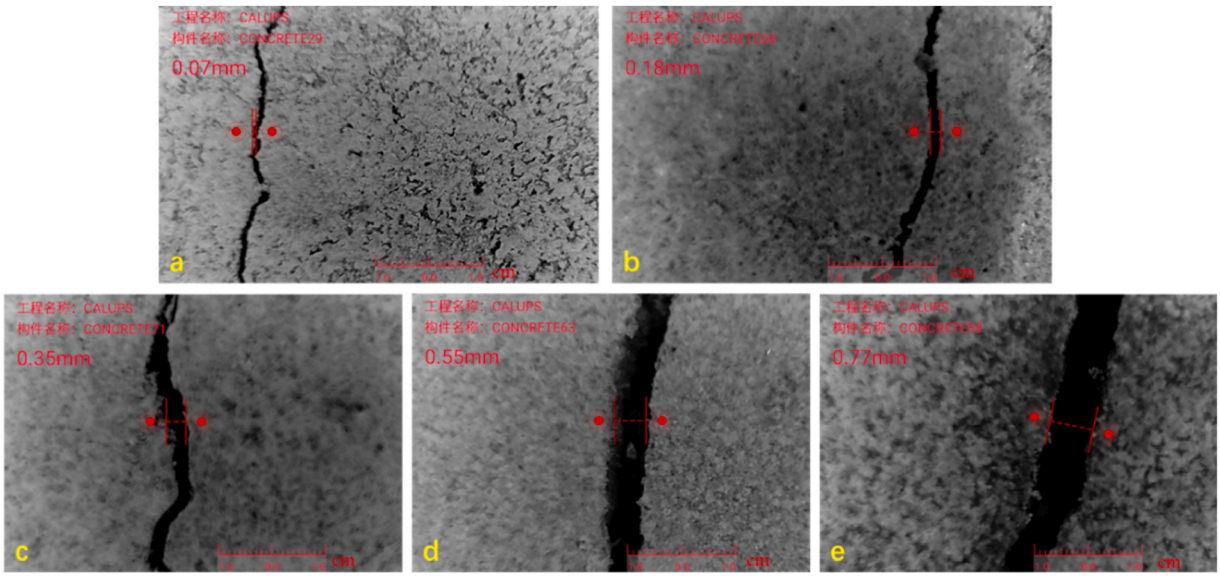

Fig. 5. Crack morphology of control groups.

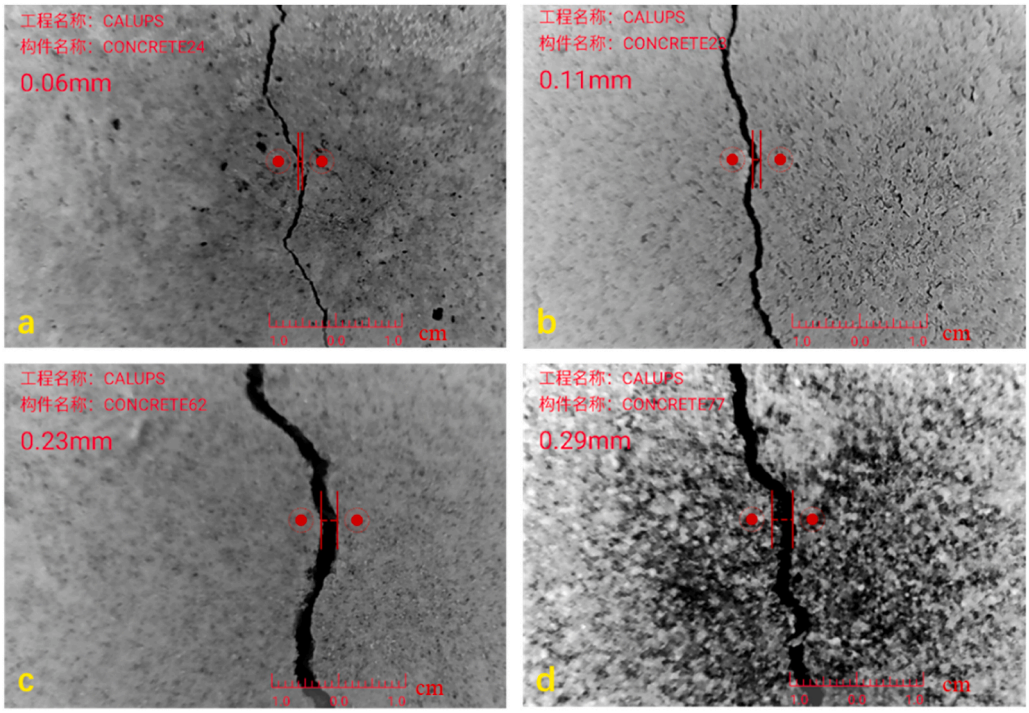

Fig. 6. Crack morphology of the experimental groups.

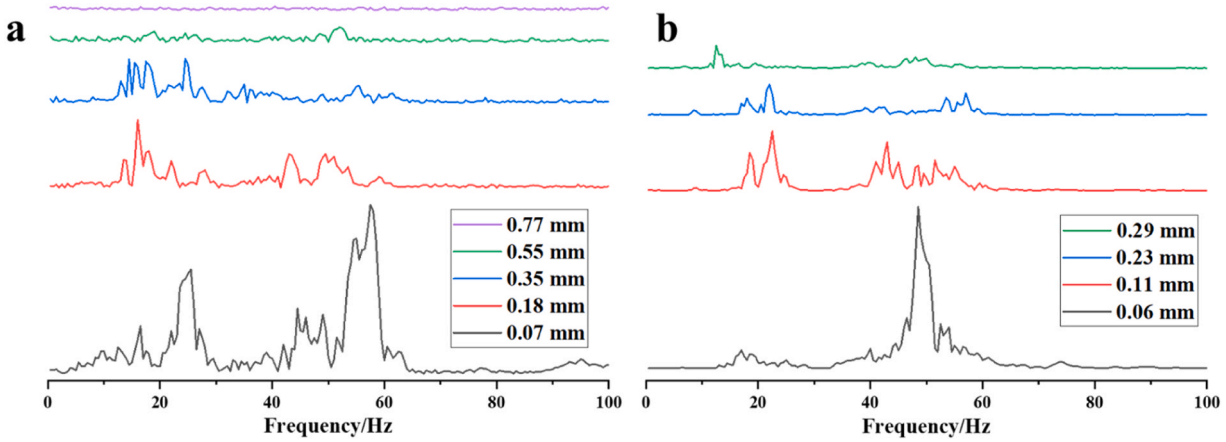

Fig. 7. Frequency domain signals under different crack widths: (a) blank groups , (b) CCCW groups.

occurred, with the primary peak migrating from 50 kHz to 20 kHz. At a critical crack width of 0.77 mm, signal detection failed entirely due to complete interfacial debonding and energy dissipation.

The monitoring of signal evolution during curing and repair processes, as shown in Figs. 8 and 10. At the same time, the amplitude of the low-frequency signal (10–30 kHz) and the amplitude of the high-frequency signal (40–60 kHz) are extracted as shown in the Figs. 9 and 11 for a clearer display of the changes. The results revealed distinct behaviors between the control and CCCW groups. For cracks below 0.1 mm, both groups exhibited no frequency shift in initial signals, with dominant peaks remaining within the 50 kHz band (Figs. 8a and 10a). In the control group, signal amplitudes initially increased during the first 7 d of curing due to progressive hydration and strength development. However, the signal amplitude decreased after 7 d and the main peak exhibit frequency shift after 7 d (Fig. 9a). These indicate that the crack deterioration caused by insufficient water at the late curing stage. This main frequency migration (from 50 kHz to around 20 kHz) reflects the physical mechanism whereby high-frequency signals (short wavelengths) undergo refraction or scattering at crack interfaces, attenuating into lower-frequency components to bypass defects. Compared with the control group, the CCCW group maintained stable signal profiles throughout the curing period, demonstrating sustained self-healing.

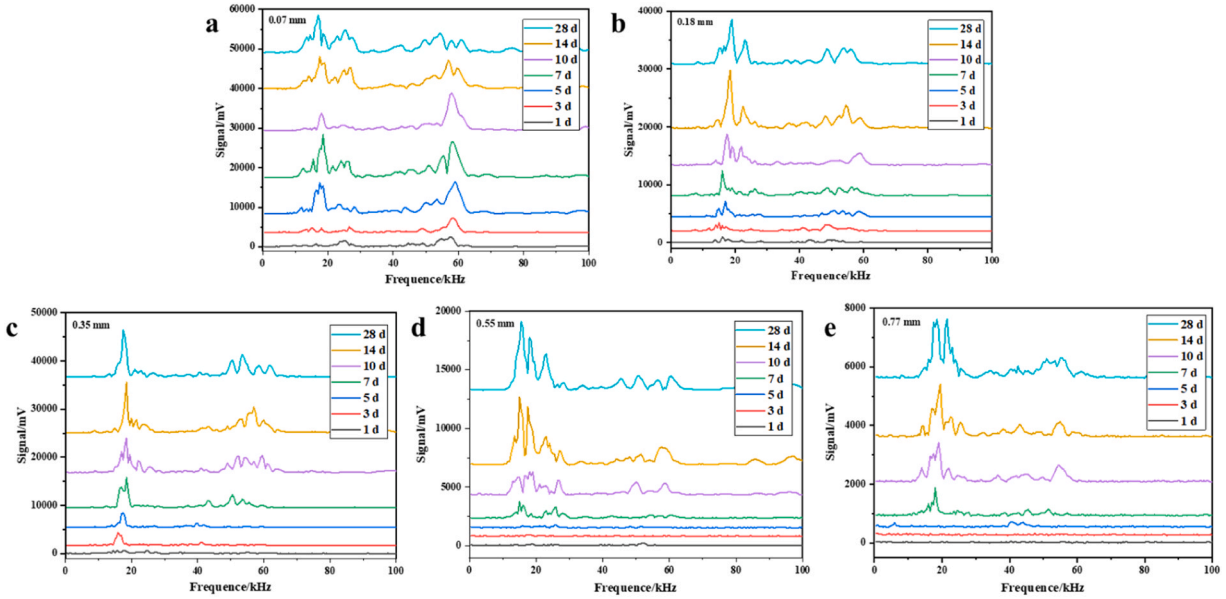

Fig. 8. Frequency domain signal changes of blank groups.

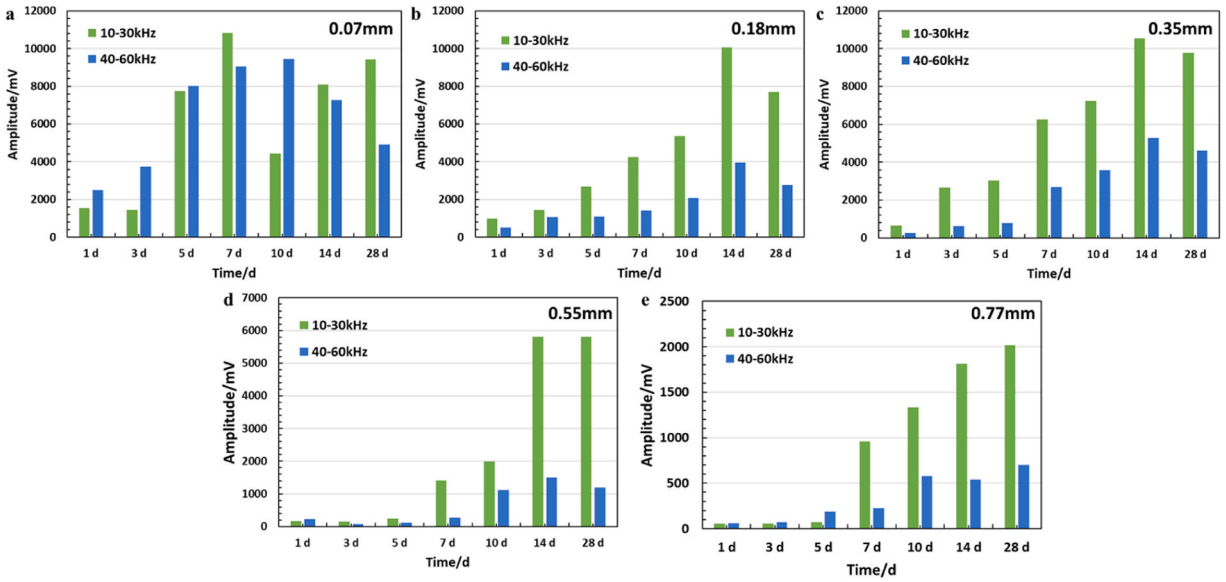

Fig. 9. Variations in signal amplitude across different frequencies (blank groups).

In the control group (Fig. 8), a significant frequency shift in the initial signal peak was observed when the crack width reached 0.18 mm. Beyond 0.55 mm, the initial signal became undetectable. As curing time progressed, the signal amplitude continued to increase, though this enhancement was exclusively localized to the low-frequency spectral band (Fig. 9). This can be attributed to the progressive strength gain of the concrete matrix. Moreover, with the extension of curing time, the frequency shift phenomenon did not improve.

In the CCCW group, similar to the control group, initial signal frequency shifts toward lower bands were observed for crack widths exceeding 0.1 mm. For cracks below 0.1 mm, the spectral profile fully recovered to a monomodal peak after 28 d of curing (Fig. 10a), closely matching the emitted signal's frequency distribution in Fig. 2b, indicating a high degree of self-healing. The healing process for 0.11 mm cracks is similar to that of 0.06 mm cracks, with post-28-day spectra displaying near-complete monomodal characteristics (Fig. 10b and Fig. 11b), although with marginally elevated low-frequency amplitudes compared to Fig. 11a. For 0.23 mm cracks, while initial frequency shifts occurred, prolonged curing enabled partial crack closure, restoring the dominant peak to the original excitation band (50 kHz) (Fig. 11c) after curing for 10 d. After 28 d, the spectral morphology approximated that of 0.06 mm cracks at 14 days,

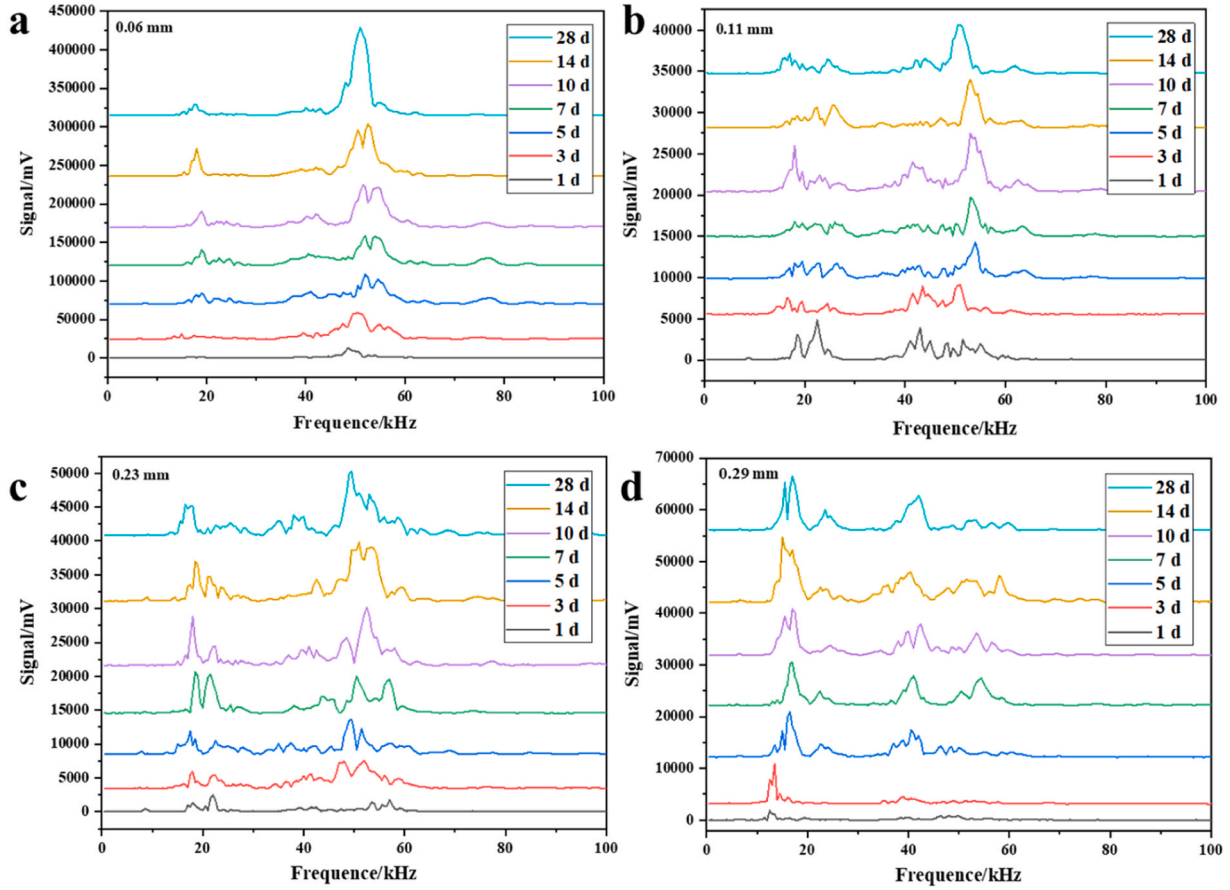

Fig. 10. Frequency domain signal changes of experimental groups.

suggesting the 0.23 mm cracks could be healed to sub-0.1 mm widths.

At 0.29 mm crack width, the main peak is difficult to restore to the original excitation frequency band. As shown in Fig. 11d, the initial signal predominantly featured low-frequency components. However, after several days healing the signal revealed progressive amplification of high-frequency amplitudes, with enhancement higher than control group counterparts at equivalent crack widths. This disparity underscores CCCW's superior crack-bridging capacity through accelerated crystalline precipitation (XRD-verified $CaCO_3$ and C-S-H formation).

The cracks in the blank groups and CCCW groups after 14 d of curing are shown in Fig. 12 and Fig. 13. In the blank group, even after 14 d of curing, no repair traces were observed on the surface of cracks below 0.1 mm (Fig. 12a, b). For larger cracks, a small amount of hydration products is formed inside, but it is insufficient to achieve the self-healing (Fig. 12c, d). In CCCW groups, it can be observed that the smaller cracks are filled with crystalline products, leading to their complete healing (Fig. 13a, b). This is also the reason why the signal in the spectrum is restored to an approximately high-frequency unimodal pattern. For wider cracks (Fig. 13c, d), although complete healing cannot be achieved, a significant amount of crystalline products form bridges across them. This bridging effect reduces leakage and contributes to a certain degree of self-healing.

Monitoring frequency shift phenomena within designated spectral bands provides a reliable means of evaluating the effectiveness of concrete crack healing. At a transmission frequency of 50 kHz, the critical threshold for observable frequency shifts is approximately 0.1 mm crack width. This threshold cannot be fully quantified through width alone, as it is inherently influenced by the coupled relationship between crack width and length. Notably, in the CCCW-modified group, 0.23 mm cracks demonstrated significant improvement in frequency shift characteristics after self-healing, whereas in the control group, even subcritical cracks (<0.1 mm) exhibited progressive deterioration and frequency shifts over extended curing periods. This contrast highlights CCCW's dual role in repairing larger cracks through crystalline bridging and mitigating late-stage microcrack propagation.

3.3. Self-healing mechanism of CCCW

According to XRF analysis, the primary chemical constituents of CCCW include CaO, MgO, SiO_2, Al_2O_3, Fe_2O_3, and Na_2O. Combined XRD and thermogravimetric (TG) analyses provide precise identification of the crystalline phases formed by these components. As shown in the XRD pattern and XRF results of CCCW (Fig. 14 and Table 8), the material is cementitious, comprising phases such as alite

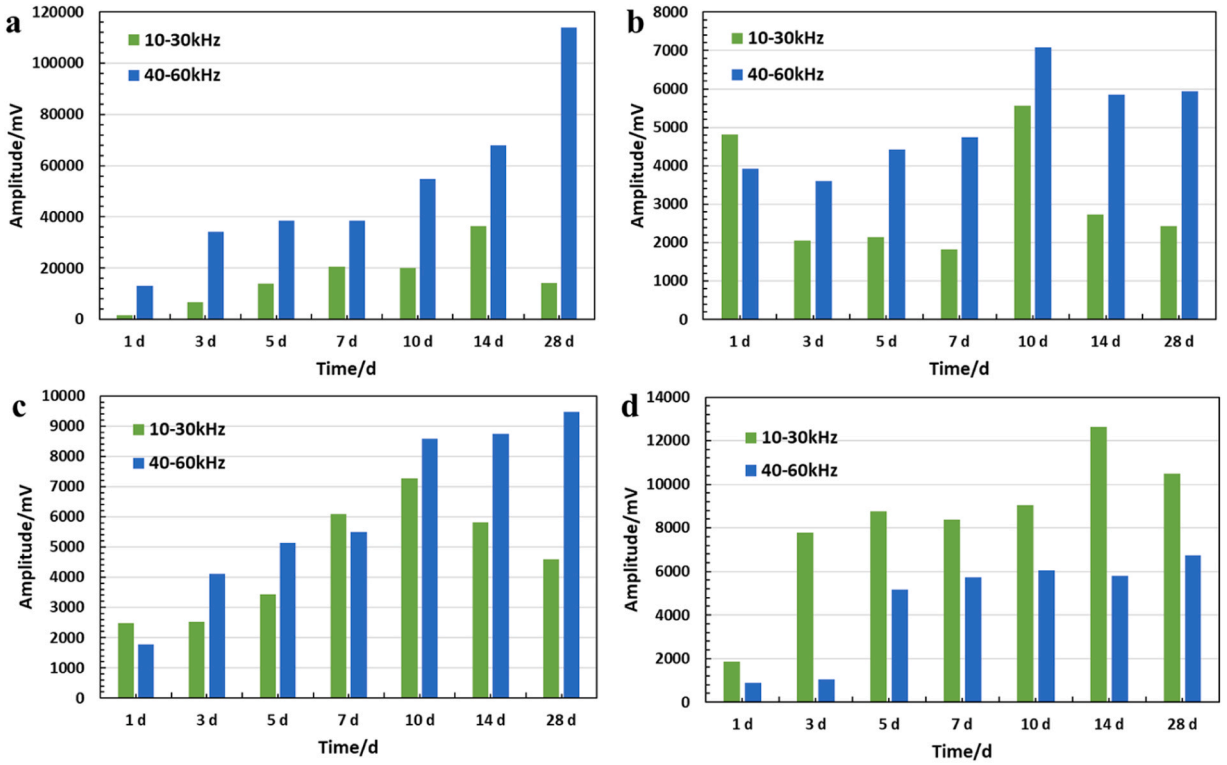

Fig. 11. Variations in signal amplitude across different frequencies (CCCW groups).

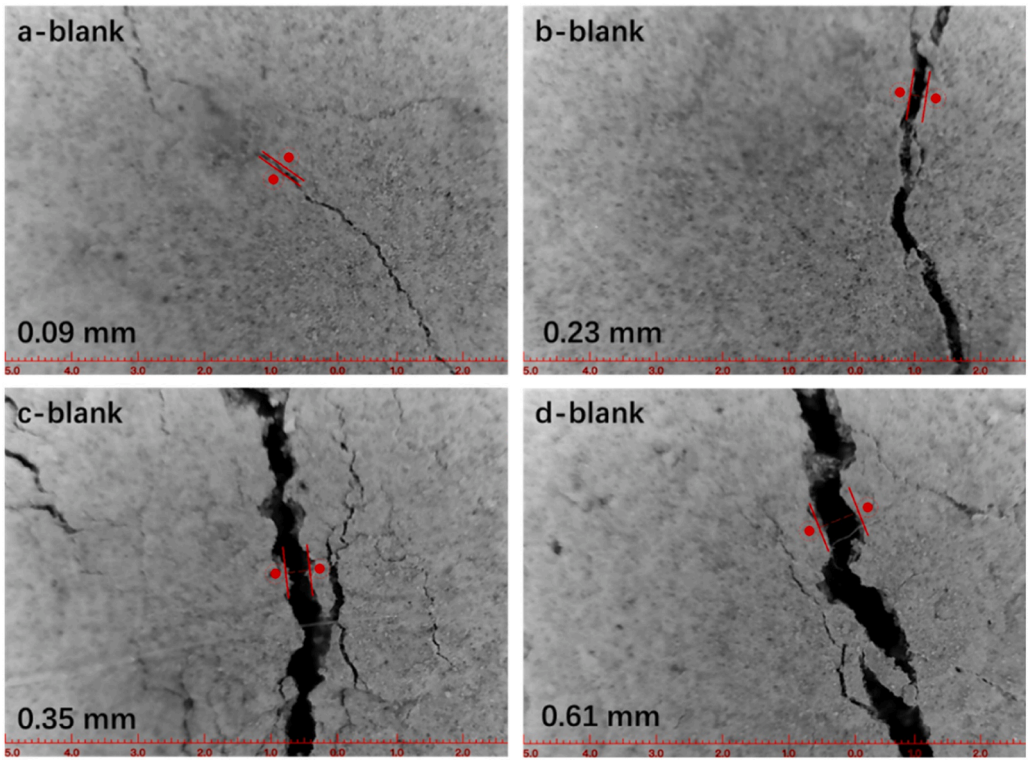

Fig. 12. The cracks in blank groups after 14d curing.

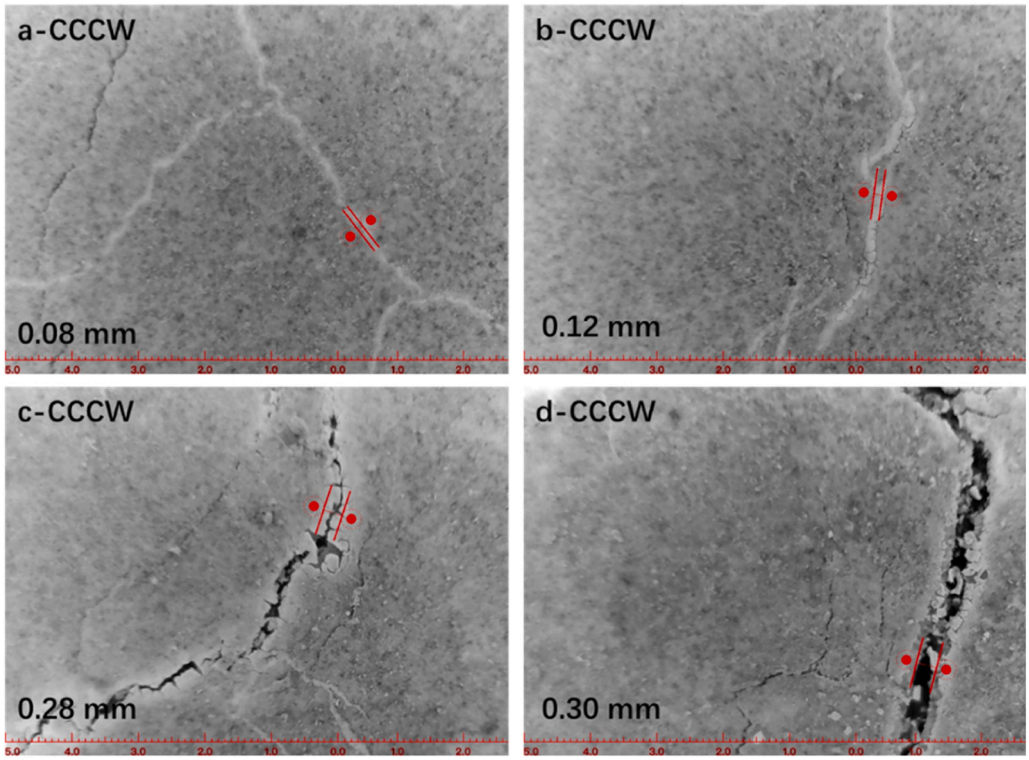

Fig. 13. The cracks in CCCW groups after 14d curing.

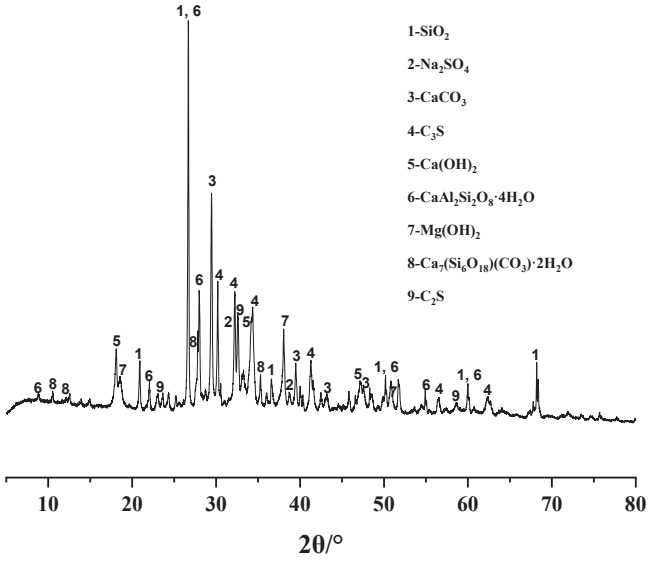

Fig. 14. The XRD pattern of CCCW.

Table 8
The XRF results of CCCW (wt%).

CaO	MgO	SiO_2	MnO	Al_2O_3	Fe_2O_3	SO_3	Na_2O	K_2O
37.40	10.47	9.56	6.23	2.15	1.94	1.91	1.19	0.19

(C_3S), quartz (SiO_2), portlandite ($Ca(OH)_2$), and calcium carbonate ($CaCO_3$), which exhibit high compatibility with concrete matrices. Additionally, CCCW contains sodium sulfate (Na_2SO_4), brucite ($Mg(OH)_2$), calcium aluminosilicate hydrate ($CaAl_2Si_2O_8{\cdot}4H_2O$, i.e., gismondine), and minor amounts of scawtite ($Ca_7(Si_6O_{18})(CO_3){\cdot}2H_2O$).

The thermogravimetric (TG) results shown in Fig. 15 further confirm the presence of the primary crystalline phases identified in CCCW. Sodium sulfate (Na_2SO_4), highly hygroscopic under ambient conditions, exists as sodium sulfate decahydrate ($Na_2SO_4{\cdot}10H_2O$), leading to a distinct dehydration peak below 100°C. Subsequent mass loss stages are attributed to sequential thermal decomposition processes: between 250°C and 500°C, the first mass loss step corresponds to the decomposition of $Mg(OH)_2$, followed by the dehydration of $CaAl_2Si_2O_8{\cdot}4H_2O$. A pronounced mass loss observed from 500°C to 650°C marks the dehydroxylation of $Ca(OH)_2$, while high-temperature mass losses above 650°C arise from the thermal decomposition of Na_2SO_4 and $CaCO_3$ [27].

The experimental results above indicate that the CCCW initially exhibits significantly improved early volume stability in concrete. Combined with XRD and SEM results (Figs. 16–18), it can be observed that, the content of $Ca(OH)_2$ significantly increased in the early curing stage (3 d) in the group with 2 % CCCW addition. Additionally, sulfate ions promoted the formation of ettringite in the CCCW group, which is evident from the increased intensity of the low-angle ettringite diffraction peak in XRD patterns. SEM images further reveal the formation of larger aspect ratio ettringite crystals in the CCCW group in the early stages, consistent with the XRD results. The larger aspect ratio of the ettringite crystals hinders the formation of wide cracks, unlike in the control group during the slab test. This structural characteristic is the primary reason for the significantly improved early-stage volume stability of CCCW group. After 28 days of curing, no further change in ettringite crystals was observed in the cement matrix, and instead, the calcium carbonate content increased due to the carbonation of excess $Ca(OH)_2$.

Monitoring experiments further demonstrated that CCCW possesses a certain self-healing capability within concrete. In the mortar specimen tests, a control group was established for comparison. After one day of curing, both the blank and CCCW groups were demolded and intentionally fractured. The specimens were then kept moist and cured for an additional five days. Crystalline products from the cracks were collected and analyzed, with the XRD results shown in the Fig. 19. The analysis reveals that the main crystalline products found in the cracks of the CCCW group are $CaCO_3$, C-S-H gels, and $Ca(OH)_2$, all of which exhibit significantly stronger diffraction peaks compared to the blank group.

These results suggest that the healing effect arises primarily from two mechanisms: (1) the deposition of hydration products, and (2) the carbonation of excess hydration products leading to the formation of $CaCO_3$. This carbonation process also facilitates the release of calcium ions, thereby promoting continued hydration. The increased generation of hydration products is attributed to the presence of organic complexing agents in CCCW [28]. These agents can form complexes with calcium ions. In the presence of water, the calcium complexes can participate in ion exchange reactions with anions such as SiO_3^{2-}, AlO_3^{2-}, and CO_3^{2-}. This reaction results in the formation of more stable calcium silicate hydrate (C-S-H) gels and $Ca(OH)_2$ crystals [29]. The diffraction peaks of C-S-H observed in the CCCW group's XRD pattern further confirm the formation of highly crystalline hydration products.

4. Conclusion

This study proposed a self-healing concrete mix design method suitable for practical engineering applications. The basic mechanical properties and durability of the concrete were tested, and its self-healing performance was evaluated using non-destructive testing methods. The main conclusions are summarized as follows:

1. By optimizing the proportions of water-reducer, expansive agent, air-entraining agent, CCCW, and fiber, crack-resistant self-healing concrete was prepared, which was suitable for anti-seepage engineering and similar applications. The compressive strength was designed in accordance with the specified strength grade, maintaining the strength redundancy coefficient below 1.2 (C45–2:

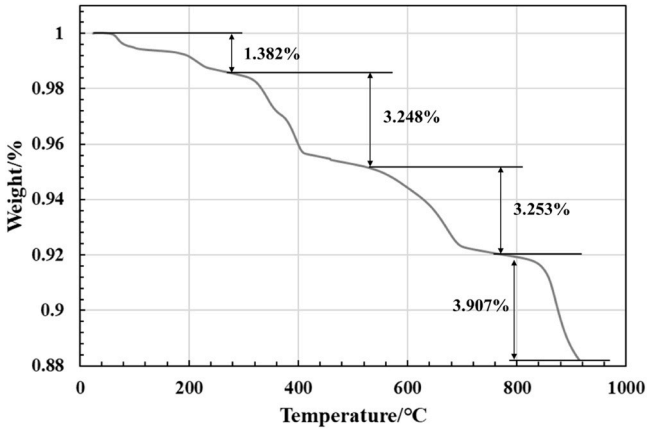

Fig. 15. The TG pattern of CCCW.

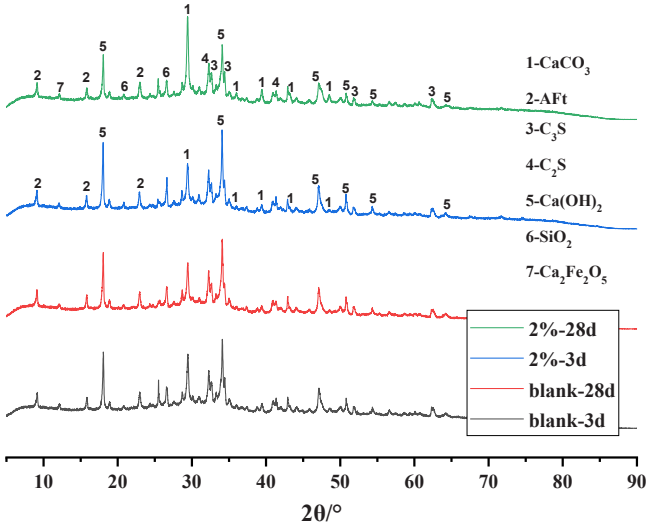

Fig. 16. XRD patterns of concrete with and without CCCW.

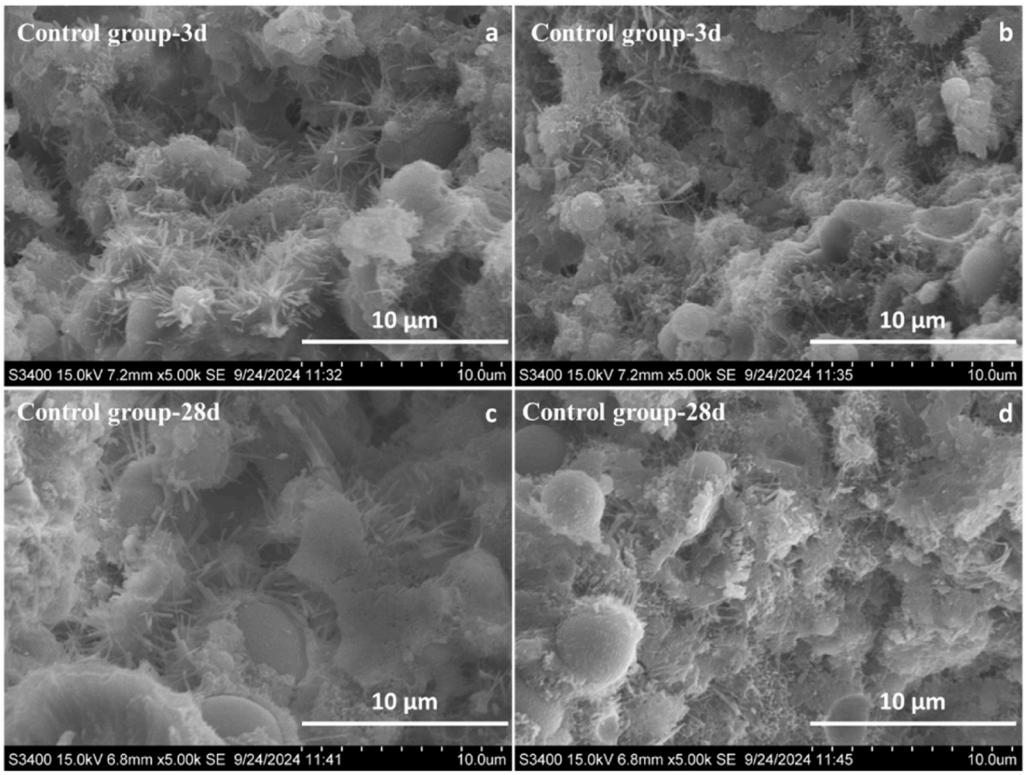

Fig. 17. SEM pictures of concrete without CCCW.

47.5 MPa for 28d). The excellent durability performance was evidenced by the absence of strength loss after 300 freeze-thaw cycles.

2. The self-healing performance of the concrete after cracking was evaluated through non-destructive testing. Based on the observed degradation and recovery patterns in frequency shifts during the healing process, it was concluded that cracks smaller than 0.2 mm can be fully healed by CCCW. For wider cracks, the formation of abundant crystalline products within the crack can significantly reduce the risk of leakage. The underlying mechanism lies in the reaction of CCCW's active components with available moisture to form $Ca(OH)_2$, C-S-H gels, and $CaCO_3$, thereby establishing an effective self-healing process.

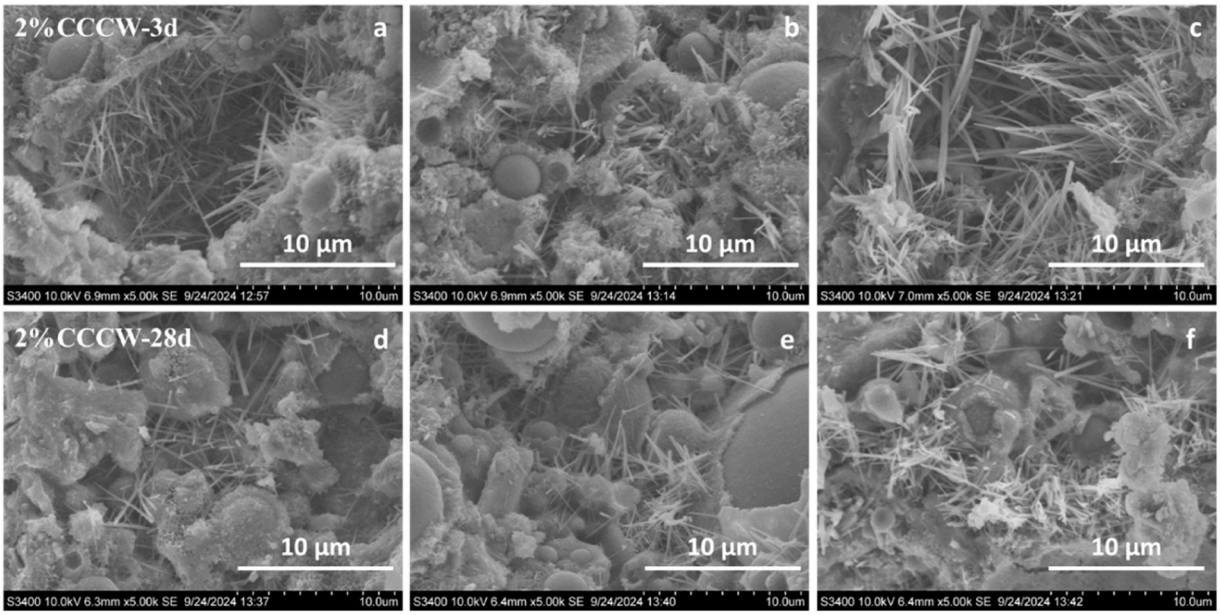

Fig. 18. SEM pictures of concrete with CCCW.

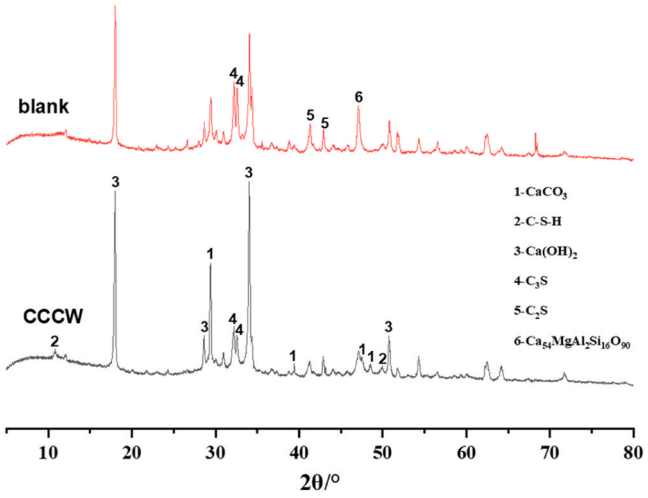

Fig. 19. XRD pattern of products inside the cracks.

CRediT authorship contribution statement

Chen Liu: Writing – review & editing, Supervision, Methodology, Formal analysis. **Baiyu Shang:** Investigation. **Zheng Zhang:** Methodology, Investigation. **Weifu Wan:** Investigation. **Yongchao Zheng:** Methodology. **Liying Jiao:** Writing – review & editing, Writing – original draft, Methodology, Investigation. **Sixue Zhao:** Writing – review & editing, Writing – original draft, Methodology, Investigation, Formal analysis, Data curation, Conceptualization.

Declaration of Competing Interest

The authors declare that they have no known competing financial interests or personal relationships that could have appeared to influence the work reported in this paper.

Acknowledgements

This work was supported by the key scientific research projects of BBMG Corporation (B20234001) and Tianjin Municipal Commission of Housing and Urban Rural Development Science and Technology Project (2025-k-10).

Data availability

Data will be made available on request.

References

[1] Ch Fu, Q. Zhan, A. Wang, et al., Study on improving the activity of mineralized microorganisms by regulating the chemical environment of marine concrete crack area with inorganic minerals, Constr. Build. Mater. 344 (2022) 128173.
[2] P. He, J. Yu, R. Wang, et al., Effect of ion chelator on pore structure, mechanical property and self-healing capability of seawater exposed mortar, Constr. Build. Mater. 246 (2020) 118480.
[3] Y. Chen, Y. Xie, Study on environmental quality standards for museum cultural relic conservation, Sci. Conserv. Archaeol. (2002) 152–191. S1.
[4] S. Granger, A. Loukili, G. Pijaudier-Cabot, Experimental characterization of the self-healing of cracks in an ultra high performance cementitious material: mechanical tests and acoustic emission analysis, Cement Concr. Res. 37 (4) (2007) 519–527.
[5] P. He, J. Yu, L. Xue, et al., Effect of ion chelator on water sorption and transport behavior of unsaturated mortars with high volume fly ash and blast furnace slag, Constr. Build. Mater. 359 (2022) 129539.
[6] H. Wang, J. Dai, X. Sun, et al., Characteristics of concrete cracks and their influence on chloride penetration, Constr. Build. Mater. 107 (2016) 216–225.
[7] A.K. Das, C.K.Y. Leung, A novel deep learning-based technique for efficient characterization of engineered cementitious composites cracks for durability assessment, Struct. Concr. 26 (2024) 2107–2123.
[8] L. Zhang, M. Zheng, D. Zhao, A review of novel self-healing concrete technologies, J. Build. Eng. 89 (2024) 109331.
[9] H.M. Jonkers, A. Thijssen, G. Muyzer, Application of bacteria as self-healing agent for the development of sustainable concrete, Ecol. Eng. 36 (2) (2010) 230–235.
[10] P. He, J. Yu, L. Xue, et al., Influence of ion chelator on pore structure, water transport and crack-healing properties of cement pastes incorporating high-volume fly ash and blast-furnace slag, J. Build. Eng. 55 (2022) 104696.
[11] Y. Su, T. Zheng, C.J. Qian, Application potential of Bacillus megaterium encapsulated by low alkaline sulphoaluminate cement in self-healing concrete, Constr. Build. Mater. 273 (2021) 121740.
[12] G. Li, X. Huang, J. Lin, Activated chemicals of cementitious capillary crystalline waterproofing materials and their self-healing behavior, Constr. Build. Mater. 200 (2019) 36–45.
[13] Q. Liu, X. Shen, B. Šavija, et al., Numerical study of interactive ingress of calcium leaching, chloride transport and multi-ions coupling in concrete, Cem. Concr. Res. 165 (2023) 107072.
[14] G. Prathamesh, Sandeep Sathe, Effect of fly ash on compressive strength, carbonation and corrosion resistance of reinforced concrete: a systematic review, World J. Eng. 22 (1) (2025) 40–60.
[15] Q. Zeng, K. Li, T. Fen-Chong, et al., Determination of cement hydration and pozzolanic reaction extents for fly-ash cement pastes, Constr. Build. Mater. 27 (1) (2012) 560–569.
[16] A. Telesca, M. Marroccoli, L. Coppola, et al., Tartaric acid effects on hydration development and physico-mechanical properties of blended calcium sulphoaluminate cements, Cem. Concr. Compos. 124 (2021) 104275.
[17] X. Zhao, C. Liu, L. Zuo, et al., Investigation into the effect of calcium on the existence form of geopolymerized gel product of fly ash based geopolymers, Cem. Concr. Compos. 103 (2019) 279–292.
[18] Y. Jia, Y. Zou, Y. Jiang, et al., Effect of a Ca-rich environment on the reaction process of the MgO-activated SiO_2 system, Cem. Concr. Compos. 136 (2023) 104855.
[19] Y. Zha, J. Yu, R. Wang, et al., Effect of ion chelating agent on self-healing performance of Cement-based materials, Constr. Build. Mater. 190 (2018) 308–316.
[20] L. Ferrara, V. Krelani, F. Moretti, On the use of crystalline admixtures in cement-based construction materials: from porosity reducers to promoters of self-healing, Smart Mater. Struct. 25 (8) (2016) 084002.
[21] W. He, Q.W. Zhan, X. Zhang, et al., Study on strengthening microbial mineralization for crack repair of cement-based materials using Mg-Al-LDHs with $C_2H_3O_2^-$, Constr. Build. Mater. 475 (2025) 141140.
[22] B.N. De, E. Gruyaert, A. Al-tabbaa, et al., A review of self-healing concrete for damage management of structures, Adv. Mater. Interfaces 5 (17) (2018) 1800074.
[23] D.V.S.K. Chaitanya, S.K. Ch Naga, A review on concrete's rheological properties, World J. Eng. 21 (1) (2024) 53–70.
[24] B. Aissa, B. Madani, A new acoustically insulating fiber-reinforced lightweight concrete based on local materials and date palm waste, World J. Eng. 21 (1) (2024) 203–214.
[25] B.M. Sabah, New approach for the mix design of high-strength concretes valorization of local aggregates, World J. Eng. 21 (3) (2024) 405–412.
[26] P. Jung-Jun, Y. Doo-Yeol, Kim Sung-Wook, Benefits of using expansive and shrinkage-reducing agents in UHPC for volume stability, Mag. Concr. Res. 66 (2014) 745–750.
[27] L. Chen, Li Zhenming, Y. Guang, Mechanisms of efflorescence of alkali-activated slag, Cem. Concr. Compos. 155 (2025) 105811.
[28] T. Ahn, T. Kishi, Crack self-healing behavior of cementitious composites incorporating various mineral admixtures, J. Adv. Concr. Technol. 8 (2) (2010) 171–186.
[29] T. Sowoidnich, T. Rachowski, C. Rößler, et al., Calcium complexation and cluster formation as principal modes of action of polymers used as superplasticizer in cement systems, Cem. Concr. Res. 73 (2015) 42–50.